Draft version October 24, 2018
Preprint typeset using LaTeX style emulateapj v. 08/22/09

INSTABILITIES OF SPIRAL SHOCKS – II. A QUASI-STEADY STATE IN THE MULTI-PHASE INHOMOGENEOUS ISM

Keiichi Wada[1]
National Astronomical Observatory of Japan, Mitaka, Tokyo 181-8588, Japan
E-mail: wada.keiichi@nao.ac.jp
Draft version October 24, 2018

ABSTRACT

The "galactic shocks" (Fujimoto 1968; Roberts 1969) is investigated using a full three-dimensional hydrodynamic simulations, taking into account self-gravity of the ISM, radiative cooling, and star formation followed by energy feedback from supernovae. This is an essential progress from the previous numerical models, in which 2-D isothermal, non-self-gravitating gas is assumed. We find that the classic galactic shocks appears is unstable and transient, and it shifts to a globally quasi-steady, inhomogeneous pattern due to non-linear development of instabilities in the disk. The spiral patterns consists of many GMC-like dense condensations, but those local structures are not steady, and they evolves into irregular spurs in the inter-arm regions. Energy feedback from supernovae do not destroy the quasi-steady spiral arms, but it mainly contributes to vertical motion and structures of the ISM. The results and methods presented here are a starting point for more consistent treatment of the ISM in spiral galaxies, in which effects of magnetic fields, radiative transfer, chemistry, and dynamical evolution of a stellar disk are taken into account.
Subject headings: ISM: structure, kinematics and dynamics — method: numerical

1. INTRODUCTION

A standing spiral shock solution was first discovered in the 60s numerically in a rotating gas disk in the galactic potential with a tightly wound spiral perturbation (i.e. the "pitch angle" is very small). Since then in the most of theoretical studies on the galactic "shock" (e.g. Fujimoto 1968; Roberts 1969; Woodward 1975; Johns, & Nelson 1986; Lubow, Cowie, & Balbus 1986), the interstellar medium (ISM) is treated as a isothermal and homogeneous fluid with two-dimensional approximation, or it is modeled as a $N-$body system of small cloudlets (e.g. Tomisaka 1986). Global evolution of the spiral shock was studied in the 80s (Johns, & Nelson 1986) using time-dependent, two-dimensional (2D) hydrodynamic simulations show that spiral shocks are stable and long-standing for various pitch angles.

However, the steady, smoothed galactic shock does not consistently explain the complicated distribution of the ISM around spiral arms and the inter-arm substructures akin to so-called 'spurs' or 'feathers'[2] observed in real spiral galaxies (Elmegreen 1980; Scoville et al. 2001; Calzetti et al. 2005; La Vigne et al. 2006). Moreover, observed molecular clouds in galactic disks do not match the picture of hydrodynamic shocks in a uniform media. It was however shown by full 2D global simulations of a non-self-gravitating, isothermal gas disk that the spurs are in fact natural consequences of "wiggle" instability, which is caused by a purely hydrodynamic phenomenon, i.e. Kelvin-Helmholtz instability (Wada, & Koda 2004) (hereafter Paper I). This phenomenon was also found in Shetty, & Ostriker (2006). They also pointed out that the features only grow in the inner-most several kpc regions if self-gravity and magnetic fields are ignored.

More recently, three-dimensional (3D) response of the gas to the spiral potential was modeled using a local shearing box approximation in isothermal, MHD simulations taking into account self-gravity (Kim & Ostriker 2006), and found that the wiggle instability is suppressed by radial flapping motion of the shock.

These previous results suggest that hydrodynamic effects, self-gravity of the gas and magnetic fields play some important roles on the gas structures in a spiral potential. However, an important feature of the real ISM has been ignored; its inhomogeneous multi-phase structures. Apparently the ISM is not 'isothermal fluid', nevertheless it is assumed in most HD and MHD simulations[3]. Effects of self-gravity and magnetic fields highly depend on gaseous temperatures and phases. In this sense, an energy equation with a realistic cooling and heating processes should be solved before taking into account those effects. Local box-approximation with a shearing periodic boundary (e.g. Kim & Ostriker 2006) is not necessarily relevant for representing dynamics of the multi-phase ISM in galactic disks, because typical scales of the inhomogeneous structures of the ISM are not small enough compared to the disk size (cf. Wada, & Norman 2001, 2007; Tasker & Bryan 2006). Moreover, since grav-

[1] Department of Astronomical Science, The Graduate University for Advanced Studies, Osawa 2-21-1, Mitaka, Tokyo 181-8588, Japan.

[2] In this paper, we refer the terms 'spurs' or 'feathers' as inter-arm gas structures, which often show quasi-periodic features associated with main spiral arms. See Paper I, Shetty, & Ostriker (2006), and Kim, & Ostriker (2002) for numerical examples, and La Vigne et al. (2006) for observations. On the other hand, 'blanches' are sub-structures bifurcated from main spiral arms. They are smoother and longer azimuthal extent than spurs, which may be caused by resonances (Chakrabarti, Laughlin, & Shu 2003).

[3] Dobbs, & Bonnell (2007) recently studied gas dynamics in a spiral potential, taking into account multi-phase nature of the ISM. However, in their non-self-gravitating SPH simulations, an energy equation with realistic cooling and heating processes is not solved, alternatively warm (10^4 K) and cold (100 K) components are treated separately as isothermal gases without phase exchange.

ity is a long-range force, global, 3D simulations for the whole disk are essential if self-gravity of the gas is considered. This is also necessary for the multi-phase ISM, because the scale height and velocity dispersion are different for cold and hot gases. In 3D hydrodynamic simulations of self-gravitating gas disks with the radiative cooling, we should take into account energy feedback from stars, otherwise the cold gas disk becomes unrealistically thin and the gravitational instability is strongly affected.

Here we show, for the first time, 3D evolution of the ISM in a galactic spiral potential, taking into account realistic radiative cooling and energy feedback from stars, especially from supernovae explosions. The simulations are performed for the whole gas disks without any assumptions for symmetry. In order to ensure a high spatial resolution (10 pc), which is essential to reproduce the multi-phase ISM, we here focus on a central part of a relatively small galaxy (radius is 2.56 kpc and the maximum circular velocity is 150 km s^{-1}). However, this is large enough to see the global effect of the spiral potential on the inhomogeneous ISM. Our simulations clarify apparent discrepancy between the steady solution of "galactic shock" and the complicated, non-steady structures of the ISM in real spiral galaxies. This is a major progress from the previous simulations, and it will be a starting point for more realistic numerical models of the ISM, taking into account 'lived' stellar potential, magnetic fields, UV radiation from massive stars, and chemistry of molecules and atoms.

2. METHODS

Evolution of a gas disk (total mass is $4.3\times10^9 M_\odot$, radius is 2.5 kpc) in a fixed gravitational potential $\Phi_{\rm ext}$ is solved by an Eulerian hydrodynamic method with a uniform Cartesian grid (Wada, & Norman 2001; Wada 2001; Wada, & Norman 2007). Here we briefly summarize the numerical scheme. We solve the following conservation equations and Poisson equation in three dimensions using $512\times512\times64$ grid points with 10 pc resolution.

$$\frac{\partial\rho}{\partial t}+\nabla\cdot(\rho\boldsymbol{v})=0, \tag{1}$$

$$\frac{\partial\boldsymbol{v}}{\partial t}+(\boldsymbol{v}\cdot\nabla)\boldsymbol{v}+\frac{\nabla p}{\rho}+\nabla\Phi_{\rm ext}+\nabla\Phi_{\rm sg}=0, \tag{2}$$

$$\frac{\partial(\rho E)}{\partial t}+\nabla\cdot[(\rho E+p)\boldsymbol{v}]=\rho\Gamma_{\rm UV}+\Gamma_\star-\rho^2\Lambda(T_g), \tag{3}$$

$$\nabla^2\Phi_{\rm sg}=4\pi G\rho, \tag{4}$$

where, $\rho, p, \boldsymbol{v}$ are the gas density, pressure, velocity of the gas. The specific total energy $E\equiv|\boldsymbol{v}|^2/2+p/(\gamma-1)\rho$, with $\gamma=5/3$.

A cooling function $\Lambda(T_g)$ ($10<T_g<10^8$K) with solar metallicity, photo-electric heating by dust ($\Gamma_{\rm UV}$) and a uniform UV radiation field ($G_0=1.0$) are assumed. The hydrodynamic scheme is AUSM (Advection Upstream Splitting Method) (Liou, M., & Steffen 1993) with MUSCL (Monotone Upstream-centered Schemes for Conservation Laws). The Poisson equation is solved to calculate self-gravity of the gas using the Fast Fourier Transform (FFT).

The external potential is given by $\Phi_{\rm ext}(R,\phi,z)\equiv\Phi_0+\Phi_1+\Phi_2$:

$$\Phi_0(R,z)\equiv av_a^2(27/4)^{1/2}(R^2+a^2+z^2)^{-1/2}, \tag{5}$$

$$\Phi_1(R,z)\equiv av_b^2(27/4)^{1/2}(R^2+b^2+z^2)^{-1/2}, \tag{6}$$

$$\Phi_2(R,\phi,z)\equiv\varepsilon_0 bR^2\Phi_1/(R^2+b^2+z^2)^{3/2}\times\cos[2\phi+2\cot i\cdot\ln(R/R_0)], \tag{7}$$

where i is the pitch angle ($i=10^\circ$) of the spiral potential, and R_0 is an arbitrary constant, and $a=0.2$ kpc, $b=2.5$ kpc, $v_a=v_b=150$ km s^{-1}, and $\varepsilon_0=0.1$. The pattern speed of the spiral potential is assumed $\Omega_p=30$ km s^{-1} kpc^{-1}. For comparison, we also run models with $\Omega_p=15$ and 60 km s^{-1} kpc^{-1} and $\varepsilon_0=0.05$. However, we find no essential differences on the conclusions (see also discussion in §4).

We take into account two feedback effects of massive stars on the gas dynamics namely: stellar winds and supernova explosions ($\Gamma_\star$). We first identify cells which satisfy criteria for star formation. The criteria for each cell where star formation is allowed are: 1) The gas density is greater than a threshold, i.e. $(\rho_g)_{i,j}>\rho_c$; 2) The temperature is less than the critical temperature, i.e. $(T_g)_{i,j}<T_c$, and 3) The criteria 1) and 2) are satisfied for 10^5 yr. Here we have chosen $T_c=100$ K and $\rho_c=600$ cm^{-3}. Assuming the Salpeter Initial Mass Function with $m_u=120M_\odot$ and $m_l=0.2M_\odot$, we create test particles representing massive stars ($>8M_\odot$). Typically a few massive stars are replaced by one test particle. The initial velocity of each test particles is taken to be the same as its parent gas. The kinematics of the test particles in the external potential and the self-gravitational potential of the gas are followed by the second-order time-integration method. The stars (test particles) inject energy due to stellar winds to the cells where the stars are located during their lifetime which is approximately$\sim10^7$ yr (Leitherer et al. 1992). When the star explodes as a supernova an energy of 10^{51} ergs is injected into the cell where the test particle is located. Non-spherical 3D propagation of blast waves in the multi-phase, non-uniform ISM is then followed consistently in the hydrodynamic simulations.

3. RESULTS

Figure 1 is time evolution of the density field on $x-y$ and $x-z$ planes of the disk in the spiral potential. High density gases form two-arm spirals, and there are also substructures, i.e. "spurs", between the spirals, as seen in real spiral galaxies (Elmegreen 1980). Each spur is a non-steady structure, but spurs are always seen in our simulations (See also the *Supplemental Movie*). As discussed in previous 2D simulations (Paper I) each spur originates in a clump, whose size corresponds to observed a Giant Molecular Cloud, formed in the spiral arm. A small gradient of angular momentum in the clump is eventually enhanced, and the clump is stretched into the inter-arm region due to galactic rotation (see also Fig. 3). In the present model, the wiggle instability (Paper I) is coupled with gravitational and thermal instabilities. This causes complicated distribution of the matter coupled with the galactic rotation and tidal shear motions. In spite of these complexities, pseudo-spiral patterns roughly associated with the spiral potential are always present. Energy feedback from SNe (average su-

pernova rate is ~ 0.2 yr^{-1}) change local density and temperature of the ISM, but it does not significantly affect global structures of the spirals in the galactic plane. Note that despite the complexity, the statistical structure of the density field (probability distribution function of density) is represented by a single log-normal function over a wide density range as predicted by Wada, & Norman (2007).

On the other hand, as shown in the right panels of Figs. 1 and 2, vertical distributions of density and temperature are strongly influenced by SNe. Cold gases ($T_g < 100$ K) as well as hot gases ($T_g \sim 10^{6-7}$ K) are blown out from the disk plane to the halo, where warm ($T_g \simeq 10^{4-5}$ K) media occupy most of the volume. The cold, dense gases sometimes form loop-like structures and fall back to the disk. In the inner region $r < 1$ kpc, where a supernova rate is higher than the outer region, the halo gas is occupied mostly by the hot gases. The interaction between the disk and halo revealed here is a numerical representation of a so-called "galactic fountain" or "chimney" (Shapiro, & Field 1976; Norman, & Ikeuchi 1989). In the original idea of the galactic fountain, hot gas is spouted up into the halo from the disk, and it cools and subsequently falls back to the disk. However, our results show that not only hot gases, but also cold, dense gases are spouted up. The vertical structure is not steady, but in a long time-scale, the cold dense gas is distributed within ~ 100 pc from the galactic plane. The scale height of the gas is smaller in the central region due to the deeper gravitational potential, but effects of a spiral potential to the vertical structure are not clearly seen.

In Fig. 3, a velocity field in a disk plane ($z = 0$) at $t = 206$ Myr is shown by streamlines overlaid on an iso-density surface[1]. The streamlines are bent near the spiral arms, and they are spread into the inter-arm regions. One should note that the "spurs" at the inter-arm regions are not located along the streamlines, but rather are perpendicular to them. As already reported in 2D simulations (Paper I), the spurs move along the galactic rotation, but they are stretched by the spread flow. This implies that the observed "spurs" are not waves. It is also apparent from Fig. 3 that the density and kinematic structures are highly irregular, therefore it may not be represented by a local computational box with a periodic boundary. Global simulations, in which the whole galactic disk is calculated without assuming symmetry, are essential to understand the structure and evolution of the ISM on a kpc scale.

The spiral structure seen in Figs. 1 – 3 does not look like the typical hydrodynamic shock, in a sense that there is no clear jump of density, and it is consisted of non-steady substructures. Figure 4 demonstrates long-term evolution of density at $r = 1.2$ kpc. We see that hydrodynamic shocks are formed upstream (i.e. on the concave side of the spiral) of the minimum of the potential trough in the first 20 Myrs or so. This is indeed the galactic shock solution found in the 60s for a tightly wound spiral potential. However, these shocks do not stay at the initial positions, and move back and forth between downstream and upstream of the potential minimum until $t \simeq 60$ Myr. After this early oscillating phase, the "shocks" disappear, and a new state emerges, characterized by its stochastic nature. The standing pattern near the potential minimum is pseudo-spiral consisting of many clumps or parts of filaments. Each inclined narrow pattern seen in Fig. 4 represents a dense region orbiting circularly around the galactic center. The trajectory can be followed between the two spirals, i.e. for about $1/4 \sim 1/2$ of the galactic rotation. This means that the substructures, i.e. spurs, in the inter-arm regions are linked with the non-steady 'chaotic arms'. Contrary to the classic galactic shock solution, the chaotic arms found here are located downstream of the potential trough on average, suggesting that the ISM does not behave like a smooth fluid. Typically the width of the waves is $\Delta\phi \simeq \pi/6$. Apparently the quasi-stable structures found here are no longer 'shocks' in a hydrodynamic sense.

Finally, positions of massive "stars" overlaid on a density map at $t = 155$ Myr are shown in Fig. 6. It is clear that massive stars form clusters, most of which are distributed near the potential trough, mostly downstream, and they form spiral features. This is reasonable since the stars originate in cold, dense clouds. In real galaxies, the massive star complexes should form H II regions around them, and they illuminate the spiral structures. Our results show that the H II regions are offset to the downstream of the dust spirals, which is consistent with observations (del Rio, & Cepa 1998; Gittins, & Clarke 2004). However, as seen in Fig. 5, the spiral arms are not uniform, and positions of density peaks in the pseudo-arms are not uniquely defined. Therefore, it would be difficult to derive dynamical information such as the pattern speed of the spiral potential and the position of corotation from observational data, for example the offset between B-band and I-band arms or the dust-arms and H_α arms (del Rio, & Cepa 1998; Gittins, & Clarke 2004).

4. DISCUSSIONS

4.1. *Effect of the Pattern Speed of the Potential*

The density structure of the ISM in spiral potential can be affected by two free-parameters here: the pattern speed and strength of the spiral potential. As mentioned in §1, bifurcation features of spiral arms could be explained by Lindblad and ultraharmonic resonances (Shu, Milione, & Roberts 1973; Chakrabarti, Laughlin, & Shu 2003). This substructure of the spiral shocks (i.e. "branches") is also seen in some models in Shetty, & Ostriker (2006), but we do not see clear evidence of the resonant structures in our results regardless of presence of resonances. Fig. 6c is density distribution at $t = 61$ Myr of a model with the pattern speed $\Omega_p = 60$ km s^{-1} kpc^{-1} [2]. As same as the fiducial model (Fig. 6b), in which $\Omega_p = 30$ km s^{-1} kpc^{-1}, the density field is characterized with inhomogeneous spiral arms and spurs in the inter-arm regions. This is also the case in a model with $\Omega_p = 15$ km s^{-1} kpc^{-1} (there are no

[1] The isodensity-map is a method to represent a 3D density field by a opaque surface on which the volume density is the same.

[2] Since our disk is small and compact (the core radius R_{core} is 0.2 kpc and maximum circular velocity is 150 km s^{-1}), $\Omega(R_{core}) - \kappa/2(R_{core}) \approx \Omega(R_{core})/2 \approx v_{max}/R_{core}$ is much larger than that in the large disk models assumed in Chakrabarti, Laughlin, & Shu (2003); Shetty, & Ostriker (2006). Therefore, the pattern speed assumed here is larger than those assumed in these previous papers (8.4 and 42 km s^{-1} kpc^{-1} in Shetty, & Ostriker (2006), 21.5 and 11.5 km s^{-1} kpc^{-1} in Chakrabarti, Laughlin, & Shu (2003)).

resonances in the disk except an ILR at $R = 0.05$ kpc). In Fig. 6a, the strength of the bar is half (i.e. $\varepsilon_0 = 0.05$) of the fiducial model (Fig. 6b) with the same pattern speed. Same as the fiducial models, the complicated spiral arms are formed, but it is located more downstream than in the model with a stronger spiral potential at this moment.

The average location of the spiral arms is probably affected by relative velocity of the gas to the spiral potential and the depth of the potential. For smaller relative velocity (i.e. large Ω_p) and/or a deeper potential, the gas clouds tend to be trapped near the potential minimum. On the other hand, for smaller pattern speeds and/or a shallower potential, the clouds passes the potential minimum and decelerate. As a result, density peaks tend to be formed more downstream on average.

4.2. *For Further Reality*

In the present model, we assume a time-independent two-arm spiral potential with a constant pitch angle, whereas the resultant morphology of the gas is quite complicated and time-dependent. These features are qualitatively consistent with near-infrared and optical observations of various types of spiral galaxies (Seigar, & James 1998; Grosbol, & Patsis 1998). In spite of the flocculent appearance of dust and young stars, the old populations seen in the K-band are dominated by two-arm spirals. The pitch angles of K-band arms are distributed between 5 and 10° independent of the Hubble type (Seigar, & James 1998). The phase-offset between the potential, young stars and dust-arms in the real galaxies could be used for studying the physical origin of the spiral arms. Unfortunately, observational constraints on the offset of the spiral arms of different components are ambiguous (del Rio, & Cepa 1998), partly because the stellar and gaseous arms are not smooth, and it is hard to trace their positions, as is the case in our simulations. The distribution of the gas and massive stars are far from regular, but more complicated than the prediction of previous idealized models.

For further reality, one should take into account the non-linear gravitational coupling between the ISM and stellar potentials as well as the realistic treatment of the ISM itself. This should be achieved in self-consistent, cosmological simulations of formation of spiral galaxies. One should realize, however that even in recent simulations (e.g. Springel & Hernquist 2005; Governato et al. 2007), the mass and spatial resolutions for gas are $10^{5-6} M_\odot$ and sub-kpc, and therefore it is hard to represent the complicated multi-phase structures of the ISM in spiral galaxies as seen in the present simulations. A much higher numerical resolution is also essential to resolve the density waves in a stellar disk.

It is not clear how the magnetic fields affect the stability of the multi-phase ISM in a spiral potential. We would like to consider this problem in future 3D MHD simulations, in which realistic cooling/heating processes as well as self-gravity of the gas are at least considered.

5. CONCLUSION

The high resolution hydrodynamic simulations, taking into account self-gravity of the gas and realistic cooling and heating processes for the ISM, reveal for the first time that the galactic spiral arms of the ISM are neither hydrodynamic shock waves nor an assembly of long-lived, bullet-like cloudlets. The global spiral arms are consist of complicated time-dependent substructures from which stars can be formed, but over a long time (at least 5-6 rotational periods), they stably exist under the influence of the spiral potential. The pseudo-spiral in the multi-phase ISM is robust for energy input from the supernovae, which mainly cause the vertical non-uniform structure of cold and hot gases. The pattern speed of the spiral potential and its strength are not key parameters to alter above features.

The ISM in galactic disks has often been represented by isothermal, non-self-gravitating fluid or inelastic particles in many astrophysical simulations. Moreover, introducing a periodic boundary condition and reducing spatial dimensions were usual. However, those kinds of simplification do not necessarily represent the nature of spiral galaxies. Magnetic fields are not considered in the present simulations, but the present results suggest that even if the magnetic fields are weak, the spiral patterns can steadily exist on a global scale. Effect of magnetic fields and other important physical processes, such as UV radiation and chemistry, should be investigated based on 3D global models, as presented in this paper.

The present treatment of the multi-phase ISM could be used for direct comparison with observations, coupled with radiative transfer calculations for various observational probes (e.g. Wada, Spaans, & Kim 2000; Wada, & Tomisaka 2005). Fine structures of molecular gas associated with the spiral arms and in the inter-arm regions in external galaxies, which could be compared with the present numerical model, will be revealed by high resolution observations, e.g. by the Atacama Large Millimeter/Submillimeter Array.

The author thanks C. Norman and J. Koda for their helpful comments. This work was supported by JSPS. The numerical computations were carried out on Fujitsu VPP5000 at Center for Computational Astrophysics in NAOJ.

REFERENCES

Chakrabarti, S., Laughlin, G. & Shu, F. H., ApJ, 596, 220
Calzetti, D., et al. 2005, ApJ, 633, 871
del Rio, M. S. & Cepa, J., 1998, A&A, 340, 1
Dobbs, C. L., Bonnell, I. A., 2007, MNRAS, 376, 1747
Elmegreen, D. M. 1980, ApJ, 242, 528
Fujimoto, M., 1968, in *IAU sympo. No.29* . The publishing house of the Academy of Sciences of Armenia, Verevan, p. 453
Gittins, D. M. & Clarke, C. J., 2004, MNRAS, 349, 909
Governato, F., Willman, B., Mayer, L., Brooks, A., Stinson, G., Valenzuela, O., Wadsley, J., & Quinn, T. 2007, MNRAS, 374, 1479
Grosbol, P. J. & Patsis, P. A., 1998, A&A, 336, 840
Johns, T. C. & Nelson, A. H., 1986, MNRAS, 220,165
Kim, W. & Ostriker, E. 2002, ApJ, 570, 132
Kim, W. & Ostriker, 2006, ApJ, 646, 213
Leitherer, C., Robert, C., & Drissen, L. 1992, ApJ, 401, 596
Lin C. C. & Shu F. H., 1964, ApJ, 140, 646

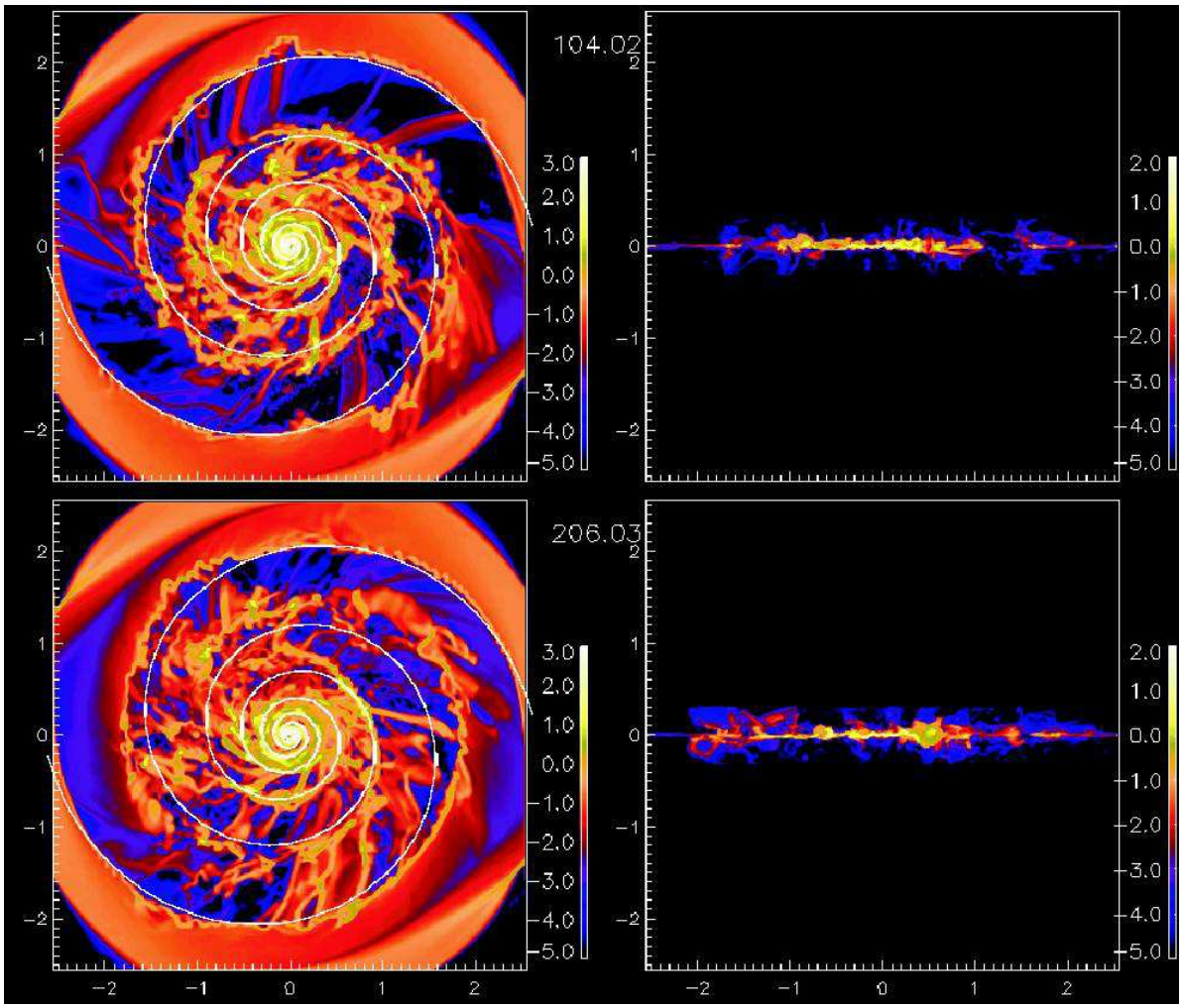

FIG. 1.— Density distribution on a galactic plane (left panels) and x-z planes (right panels) at $t = 104$ and 206 Myr from the initial condition. The color represents log-scaled density ($M_\odot$ pc^{-3}). The unit of the scale is kpc. (See also the Supplemental Movie for more detailed time evolution.)

Liou, M., Steffen, C., 1993, J.Comp.Phys., 107, 23
Lubow, S. H., Cowie, L. L. & Balbus, S. A. 1986, ApJ, 309, 496
Norman, C. A. & Ikeuchi, S. 1989, ApJ, 345, 372
Roberts, W. W. 1969, ApJ, 158, 123
Scoville, N., et al. 2001, ApJ, 122, 301
Seigar, M. S. & James, P. A., 1998, MNRAS, 299, 685
Shu, F. H., Milione, V. & Roberts, W. W., 1973, ApJ, 183, 819
Shetty, R. & Ostriker, E. C. 2006, ApJ, 647, 997
Shapiro, P. R. & Field, G. B., 1976, ApJ, 205, 762
Springel, V., & Hernquist, L. 2005, ApJ, 622, L9
Tasker, E. J., & Bryan, G.L̃., 2006, ApJ, 641, 878
Tomisaka, K., 1986, PASJ, 38, 95
La Vigne, M. A., Vogel, S. N., & Ostriker, E. C. 2006, ApJ, 650, 818
Wada, K. & Norman, C. A., ApJ, 660, 276
Wada, K., Spaans, M. & Kim, S., 2000, ApJ, 540, 797
Wada, K. & Tomisaka, K., 2005, ApJ, 619, 93
Wada, K. & Norman, C. A., 2001, ApJ, 547, 172
Wada, K., 2001, ApJ, 559, L41
Wada, K. & Koda, J., 2004, MNRAS, 349, 270 (Paper I)
Woodward, P. 1975, ApJ, 195, 61

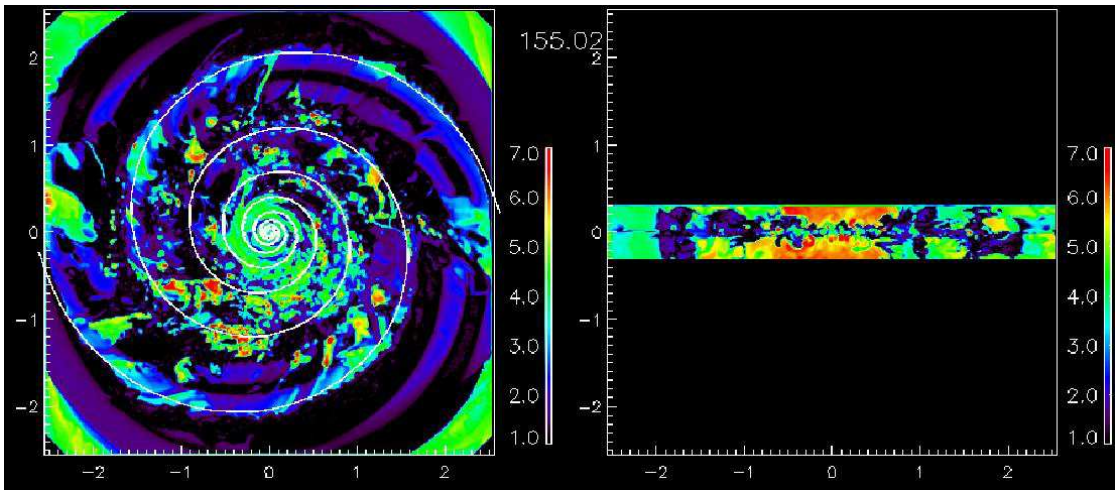

FIG. 2.— Same as Fig. 1, but for temperature distribution at $t = 155$ Myr. The color represents log-scaled temperature (K). The red regions are hot gases generated by supernovae.

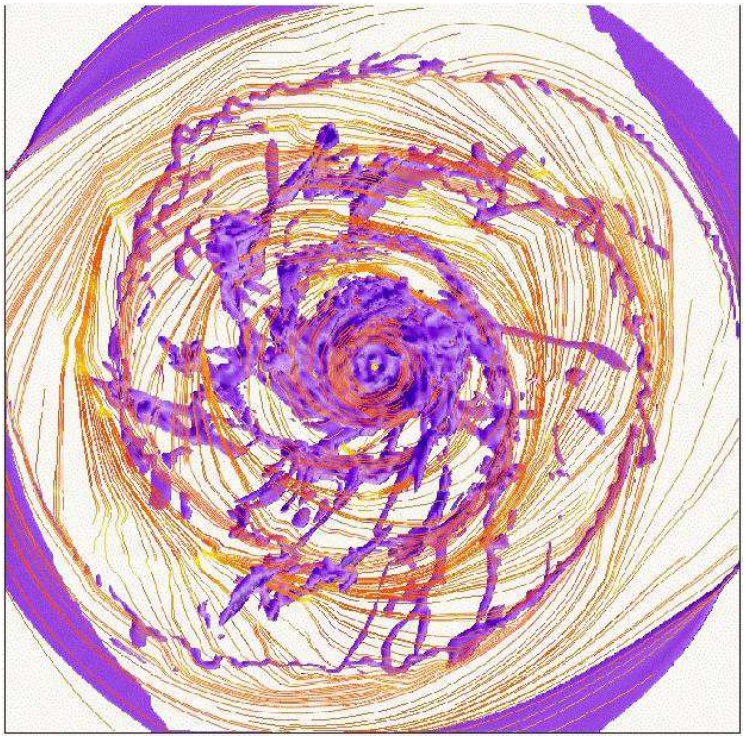

FIG. 3.— Same as Fig. 1, but for streamlines on the galactic plane ($z = 0$) overlaid on an iso-density surface ($\rho > 10^{-0.78} M_\odot$ pc$^{-3} \sim 10$ cm^{-3}) at $t = 206$ Myr. Note that the streamlines are generated by u and v components. The velocity field is non-steady, therefore the structure of the streamlines are time-dependent.

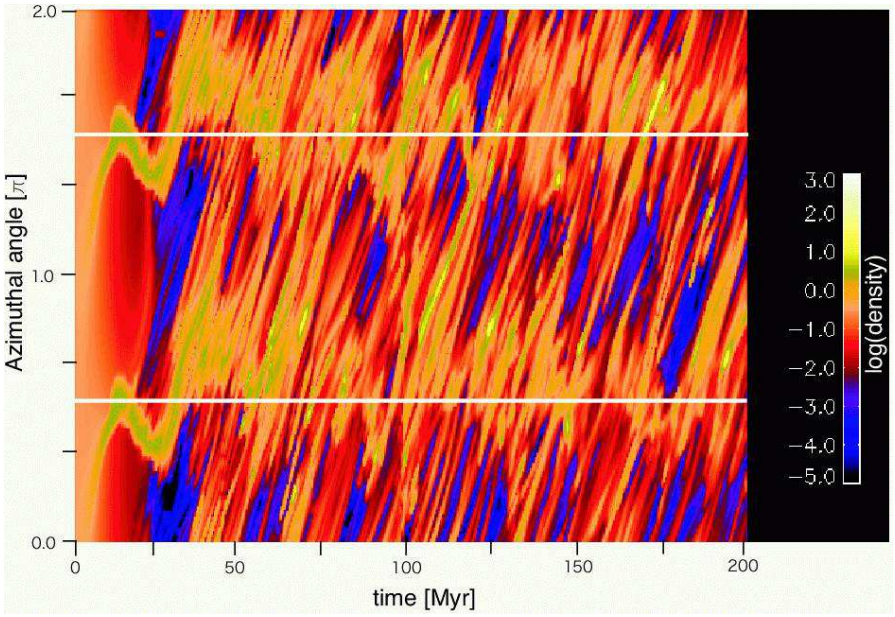

FIG. 4.— Time evolution of azimuthal density profile at $r = 1.2$ kpc. The color represents log-scaled density ($M_\odot$ pc^{-3}). The white lines show the positions of the minimum of the spiral potential. The initial 'shock' turns to be stochastic arms consisting of many substructures after $t \simeq 60$ Myr.

FIG. 5.— Position of 7.9×10^4 "massive star" particles overlaid on the density map at $t = 155$ Myr. The size of the box is 5.12× 5.12 kpc.

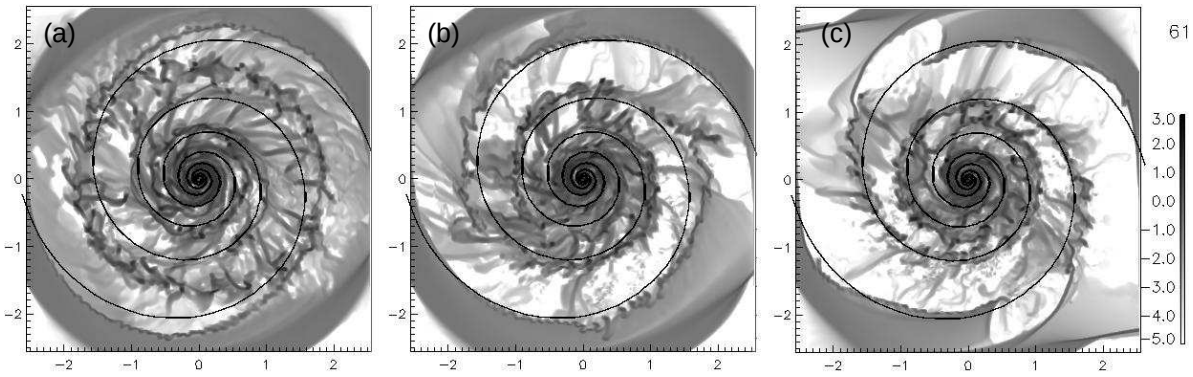

FIG. 6.— Density distributions at $t = 61$ Myr for models with (a) $\Omega_p = 30$ km s^{-1} kpc^{-1} and $\epsilon = 0.05$ (b) $\Omega_p = 30$ km s^{-1} kpc^{-1} and $\epsilon = 0.1$, (c) $\Omega_p = 60$ km s^{-1} kpc^{-1} and $\epsilon = 0.1$. Gray-scale represents log-scaled density in the unit of $M_\odot$ pc^{-3}. Radii of corotation, inner Lindblad resonances, and 4:1 ultraharmonic resonance are 2.7, 0.09, 0.74, and 1.46 kpc, respectively for (c), and 5.1, 0.05, 1.15 kpc, respectively for (a) and (b). There are no ultraharmonic resonances in the computational region for (a) and (b). There are no clear resonance-driven features (so-called blanches) at any resonance radii. There is no clear sign that time-dependent inhomogeneous substructures of spiral arms and inter-arm regions (so-called spurs) are caused by the resononances.